Supplement of Hydrol. Earth Syst. Sci., 30, 4095–4116, 2026
https://doi.org/10.5194/hess-30-4095-2026-supplement

Hydrology and Earth System Sciences
Open Access
EGU

Supplement of

Identifying dominant parameters in SWAT across subbasin and HRU scales using a two-step deep learning-assisted spatial sensitivity analysis

Jing Yang et al.

Correspondence to: Tian Jiao (tianjiao@nwu.edu.cn) and Yonghua Zhao (yonghuaz@chd.edu.cn)

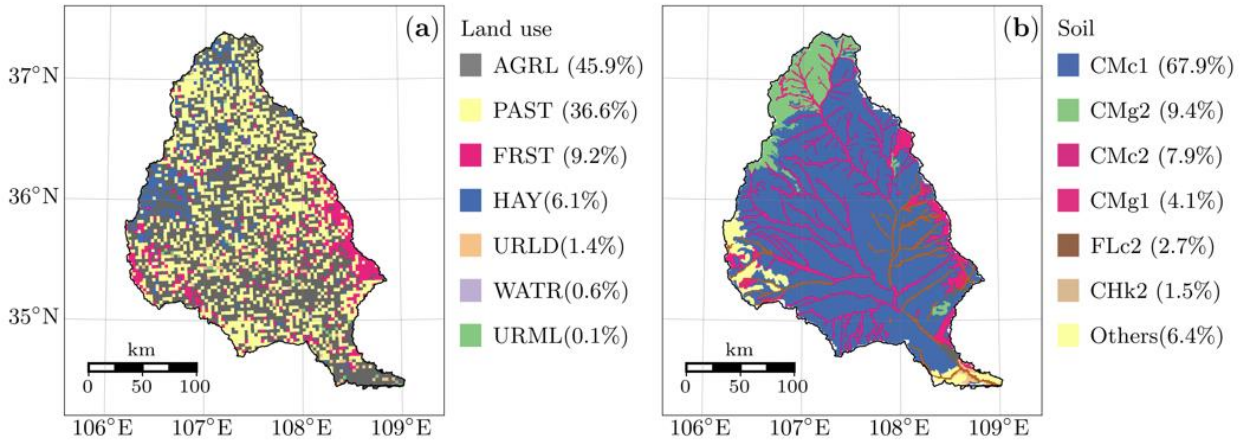

Figure S1: Classifications of (a) the resample land use (3,000 m resolution) from the 30-m Resolution Global Land Cover 2017 dataset (https://data-starcloud.pcl.ac.cn/iearthdata, accessed August 20, 2025). Categories include agricultural (AGRL), pasture (PAST), forest (FRST), hay (HAY), low-density residential (URLD), water (WATR), and medium/low-density residential (URML). (b) the soil data derived from the Harmonized World Soil Database (HWSD, 1 km resolution), provided by the National Cryosphere Desert Data Center (https://www.ncdc.ac.cn/portal/, last access: 20 August 2025). Categories include calcaric cambisols (CMc1, CMc2), calcaric regosols (CMg1, CMg2), fluvisols (FLc2), and chernozems (CHk2).

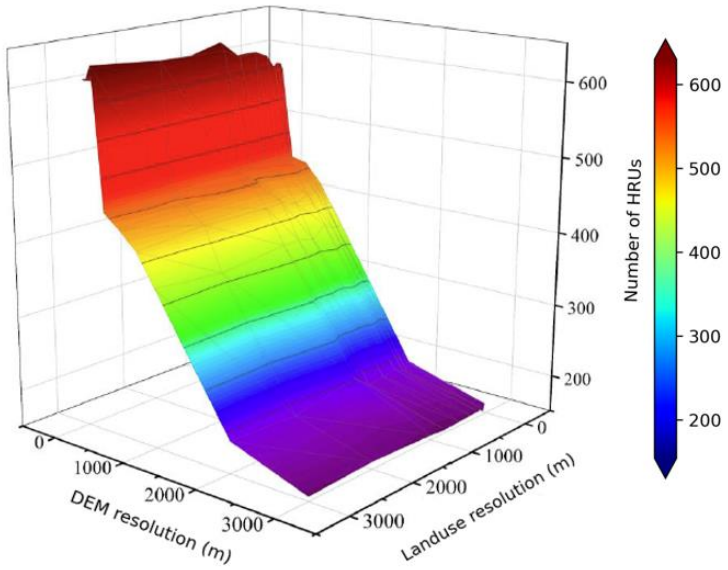

Figure S2： Number of HRUs derived from DEM and land use data at different spatial resolutions. Both DEM and land use resolutions were resampled from 30 to 3000 m (i.e., 30, 60, 90, 150, 300, 500, 750, 1000, 2000, and 3000 m), resulting in 100 different HRU delineations based on their combined configurations.

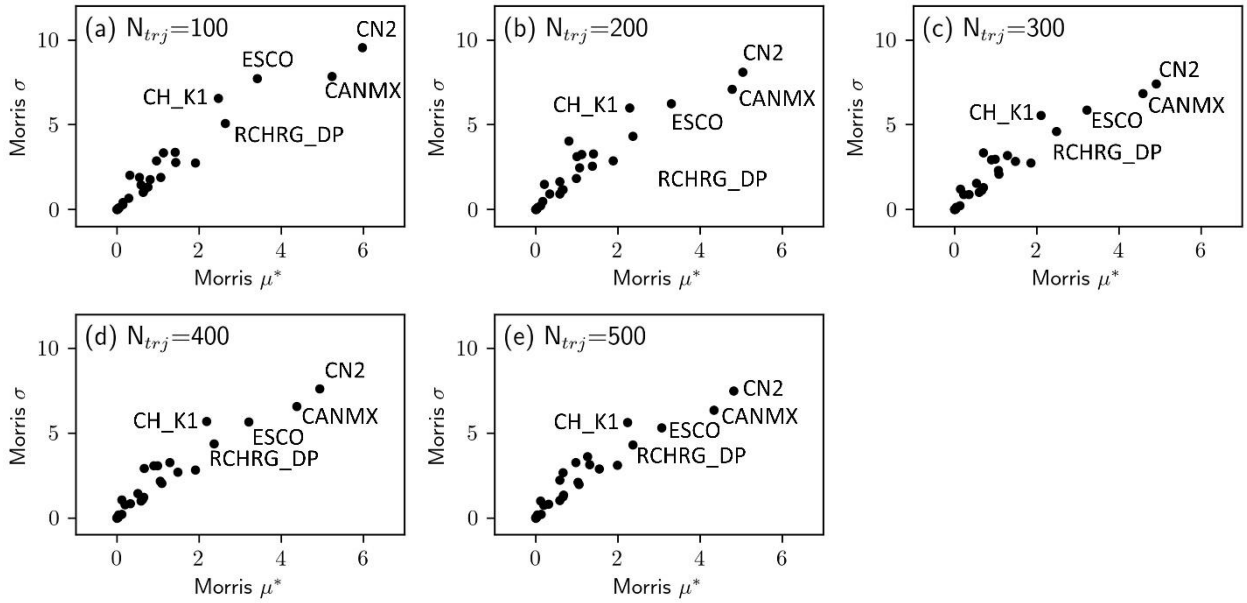

Figure S3：Morris sensitivity results obtained using different numbers of trajectories, illustrating the stability of five screened parameters across (a) 100, (b) 200, (c) 300, (d) 400, and (e) 500 trajectories.

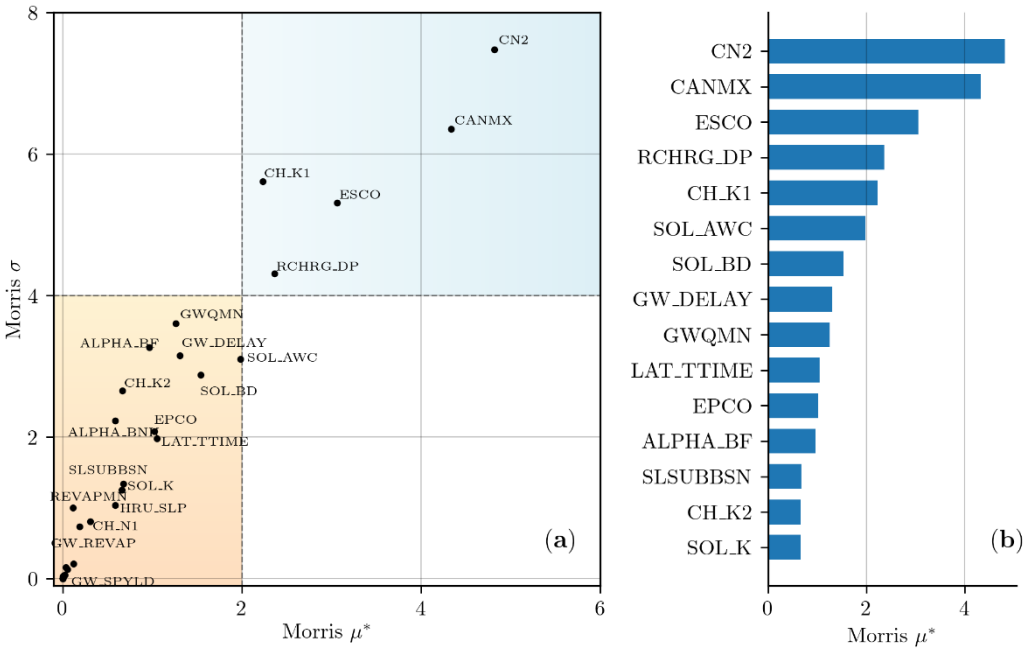

Figure S4: Sensitivity analysis results by Morris screening method for NSE-based runoff simulations at ZJS gauge station: (a) scatter plot of the mean absolute elementary effect (μ*) versus its standard deviation (σ) for 33 selected parameters. (b) bar chart ranking the top 15 parameters by μ*. Parameters with larger μ* values exert stronger overall influence on model performance, while higher σ values indicate nonlinear or interaction effects. The shaded gradient zones in panel (a) highlight regions of dominant influence: the upper-right blue zone denotes parameters with both high overall impact and strong interactions, whereas the lower-left orange zone indicates parameters with limited influence. The parameter GW_SPYLD is not active in the SWAT model, therefore, both its μ* and σ values are zero, confirming the effectiveness of the Morris method in identifying non-influential parameters.

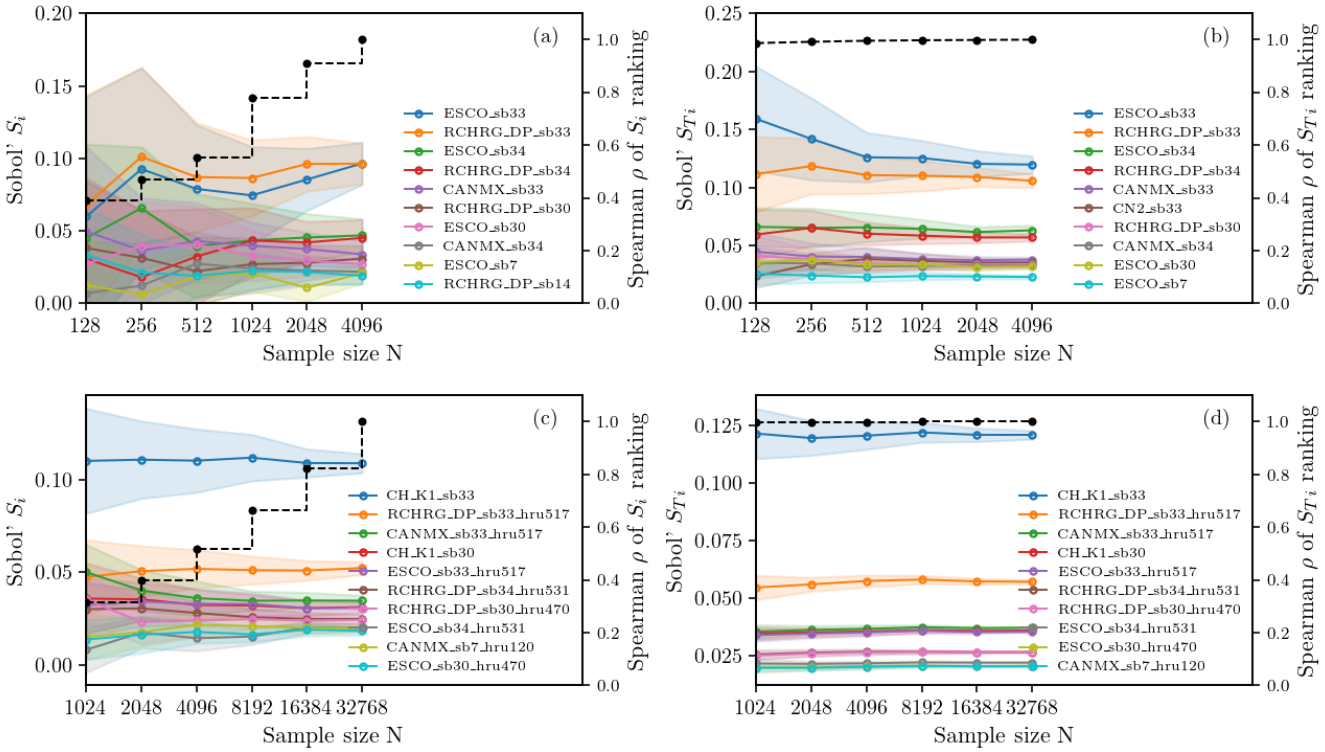

Figure S5: Convergence assessment of Sobol' sensitivity indices at subbasin and HRU scales. Panels (a) and (b) show the convergence of first-order S_i and total-effect S_{Ti} indices at the subbasin scale, respectively, while panels (c) and (d) present the corresponding results at the HRU scale. Coloured lines represent the evolution of sensitivity indices for the ten most influential parameters as a function of sample size N and shaded areas denote the associated 95% bootstrap confidence intervals. Black dashed step lines indicate the stability of parameter rankings, quantified using the Spearman rank correlation coefficient relative to the largest sample size (N = 4,096 for the subbasin scale and N = 32,768 for the HRU scale), computed across all parameters (195 at the subbasin scale and 2,559 at the HRU scale). For clarity, only the top ten parameters ranked by S_i and S_{Ti} are shown.

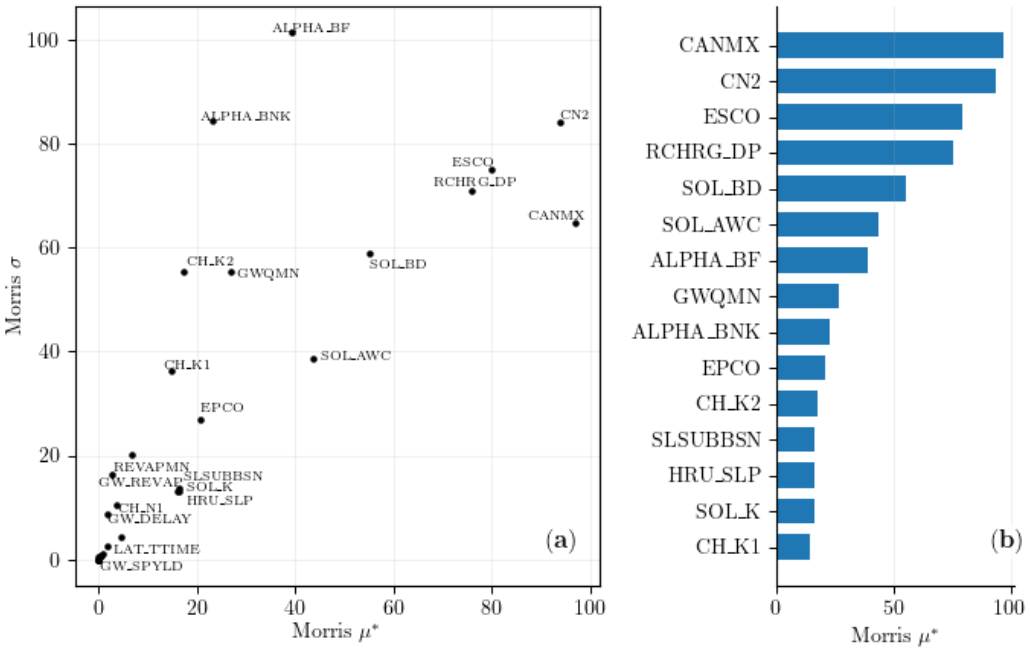

Figure S6: Sensitivity analysis results by Morris screening method for PABIS-based runoff simulations at ZJS gauge station: (a) scatter plot of the mean absolute elementary effect (μ*) versus its standard deviation (σ) for 33 selected parameters. (b) bar chart ranking the top 15 parameters by μ*.

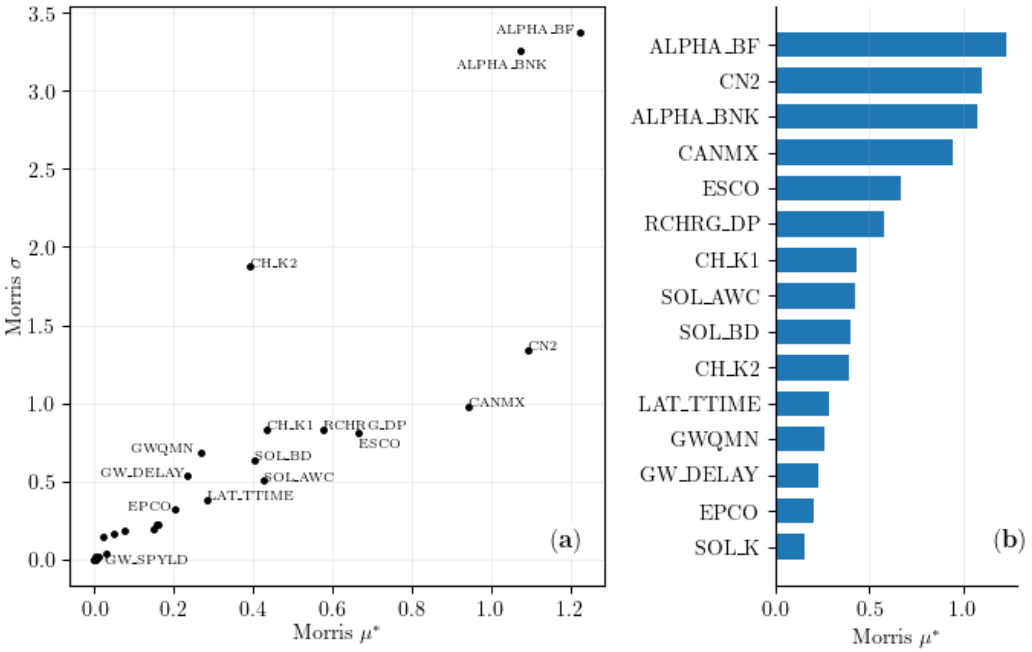

Figure S7: Sensitivity analysis results by Morris screening method for KGE-based runoff simulations at ZJS gauge station: (a) scatter plot of the mean absolute elementary effect (μ*) versus its standard deviation (σ) for 33 selected parameters. (b) bar chart ranking the top 15 parameters by μ*.

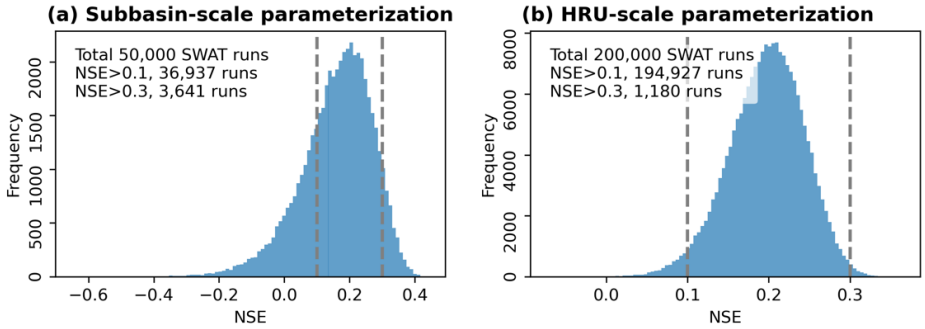

Figure S8: Histograms of NSE calculated from (a) 50,000 SWAT simulations used to construct the subbasin-scale MLP surrogate and (b) 200,000 SWAT simulations used to construct the HRU-scale MLP surrogate. The two vertical grey dashed lines indicate the NSE thresholds of 0.1 and 0.3, respectively.

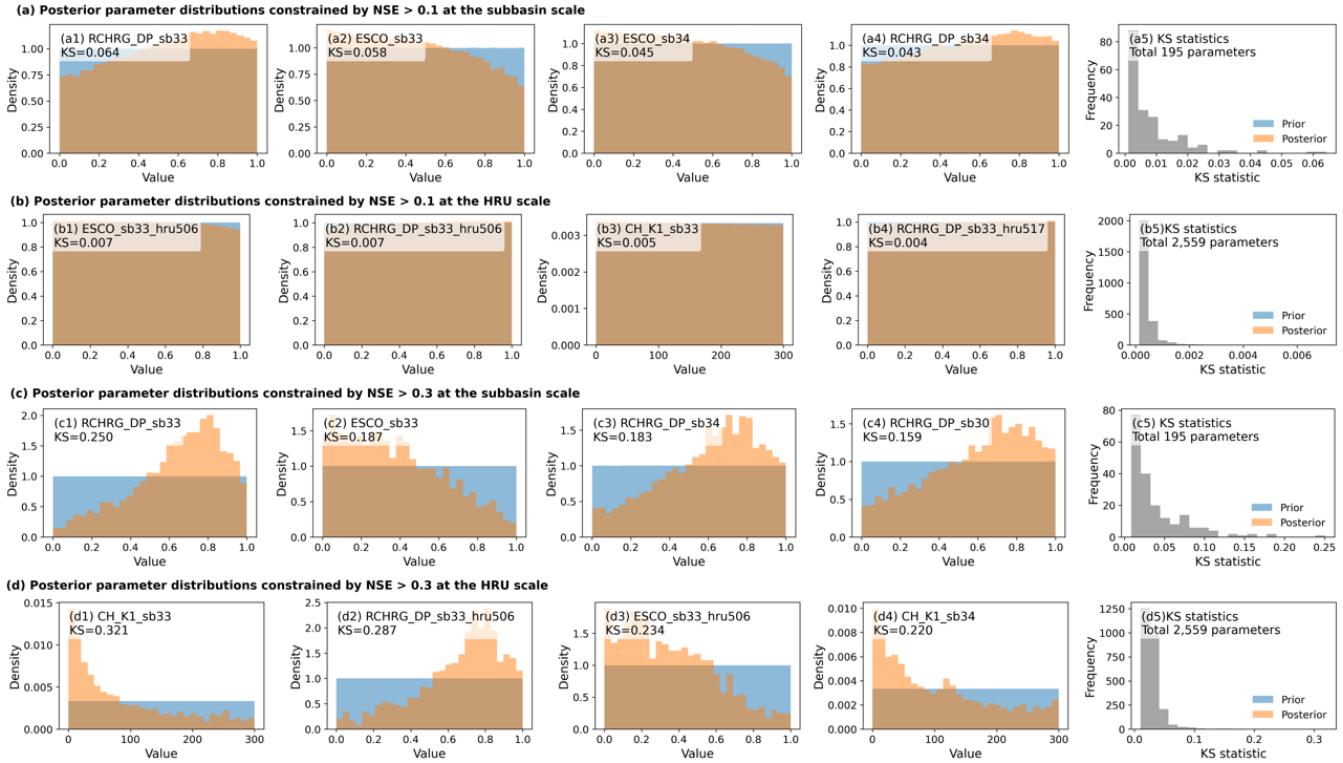

Figure S9: Comparison of the prior and posterior distributions of the four parameters exhibiting the largest Kolmogorov–Smirnov (KS) statistics, together with histograms of KS values across all distributed parameters constrained by (a) NSE > 0.1 at the subbasin scale, (b) NSE > 0.1 at the HRU scale, (c) NSE > 0.3 at the subbasin scale and (d) NSE > 0.3 at the HRU scale. KS values close to 0 indicate minimal deviation between the prior and posterior distributions, whereas values approaching 1 signify strong posterior constraints.

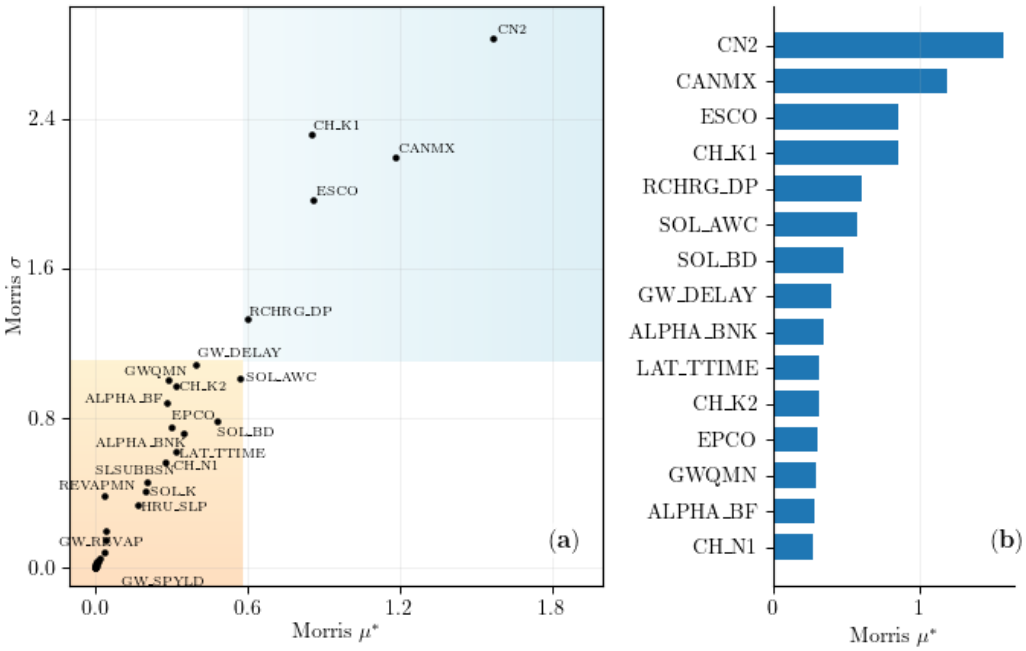

Figure S10: Sensitivity analysis results by Morris screening method for NSE-based runoff simulations at YJP gauge station: (a) scatter plot of the mean absolute elementary effect (μ*) versus its standard deviation (σ) for 33 selected parameters. (b) bar chart ranking the top 15 parameters by μ*.

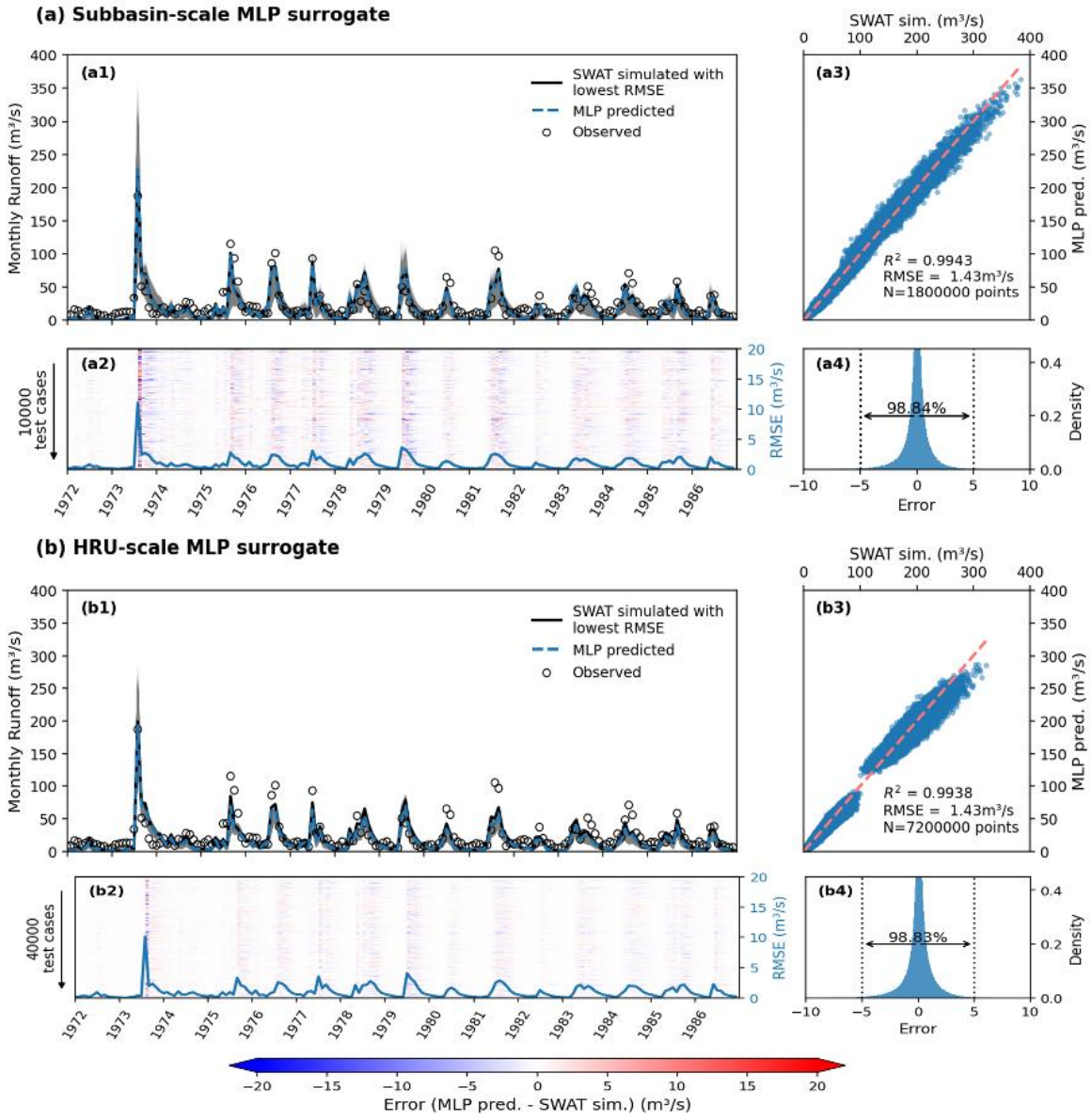

Figure S11: Performance of the trained MLP surrogates for YJP gauge station at the (a) subbasin and (b) HRU scales. Panels (a1) and (b1) compare ensemble SWAT simulations for the test cases (grey lines; 10,000 cases at the subbasin scale and 40,000 cases at the HRU scale), the specific SWAT-simulated runoff with the lowest RMSE relative to observed runoff (black lines) and the corresponding MLP-predicted runoff (blue dashed lines), as well as observed runoff (black circles) at the YJP gauge station. Panels (a2) and (b2) show heatmaps of prediction errors across 180 months from 1972 to 1986 for all test cases; blue solid lines indicate the RMSE values calculated for each month across realizations. Panels (a3) and (b3) present scatter plots of MLP-predicted versus SWAT-simulated runoff. Panels (a4) and (b4) show the error density.

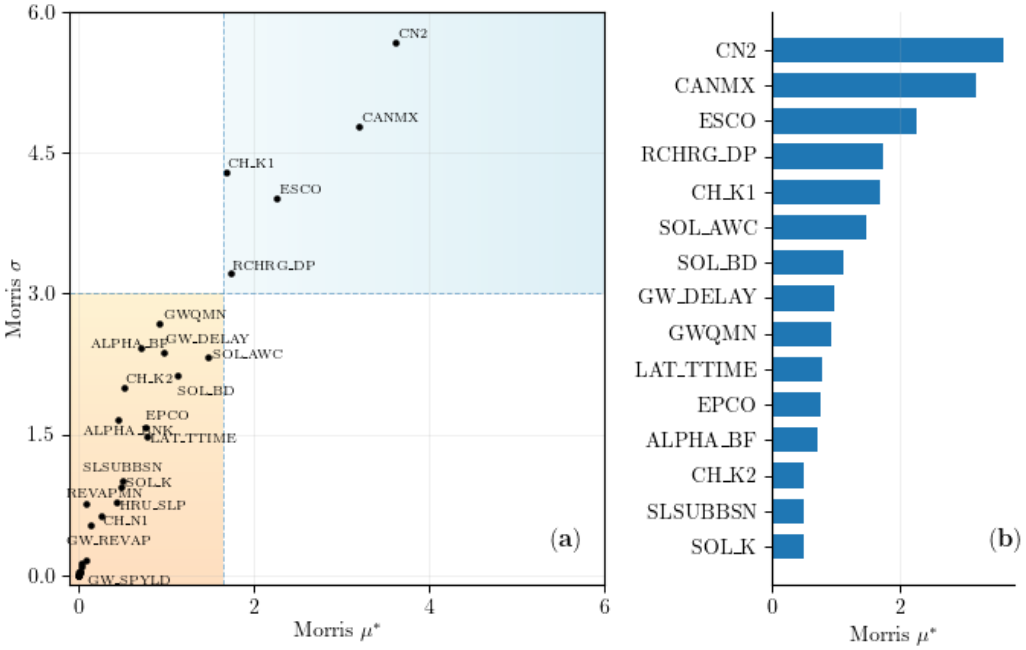

Figure S12: Sensitivity analysis results by Morris screening method for aggregated NSE across the YJP and ZJS stations: (a) scatter plot of the mean absolute elementary effect (μ*) versus its standard deviation (σ) for 33 selected parameters. (b) bar chart ranking the top 15 parameters by μ*.

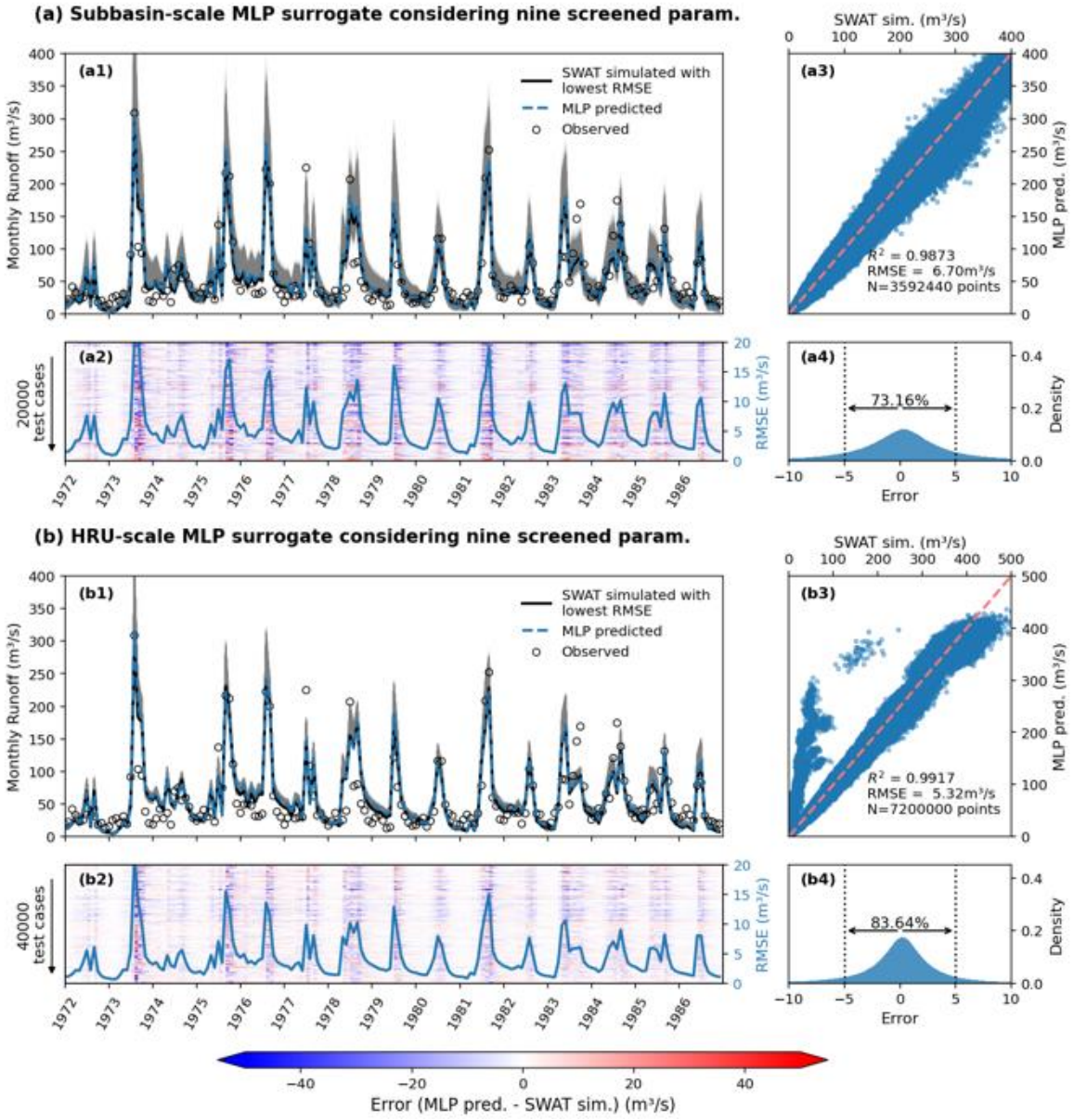

Figure S13: Performance of the trained MLP surrogates using the nine screened parameters at the (a) subbasin and (b) HRU scales. Panels (a1) and (b1) compare ensemble SWAT simulations for the test cases (grey lines; 10,000 cases at the subbasin scale and 40,000 cases at the HRU scale), the specific SWAT-simulated runoff with lowest RMSE relative to observed runoff (black lines) and the corresponding MLP-predicted runoff (blue dashed lines), as well as observed runoff (black circles) at the YJP gauge station. Panels (a2) and (b2) show heatmaps of prediction errors across 180 months from 1972 to 1986 for all test cases; blue solid lines indicate the RMSE values calculated for each month across realizations. Panels (a3) and (b3) present scatter plots of MLP-predicted versus SWAT-simulated runoff. Panels (a4) and (b4) show the error density.

Table S1: Relationship between 39 subbasins and 630 HRUs. For each subbasin, the table lists its area and the contiguous HRU ID range, which were derived from the ArcSWAT HRU Analysis Report.

Subbasin ID	Area (km^2)	HRU ID range	Subbasin ID	Area (km^2)	HRU ID range
1	2010.2	1 – 17	21	3139.8	324 – 346
2	2560.8	18 – 41	22	296.6	347 – 361
3	692.75	42 – 64	23	178.16	362 – 378
4	857.59	65 – 83	24	327.67	379 – 387
5	1765	84 – 101	25	15.57	388 – 393
6	922.77	102 – 113	26	1005.4	394 – 413
7	1714.2	114 – 123	27	1668.2	414 – 433
8	3022.1	124 – 135	28	388.87	434 – 442
9	371.99	136 – 144	29	248.92	443 – 460
10	826.02	145 – 165	30	1466.7	461 – 475
11	2412.6	166 – 194	31	95.963	476 – 487
12	928.62	195 – 203	32	927.52	488 – 504
13	280.24	204 – 213	33	2430.7	505 – 521
14	3370.4	214 – 231	34	1931.6	522 – 532
15	981.13	232 – 251	35	1256.5	533 – 555
16	801.04	252 – 270	36	929.68	556 – 577
17	151.16	271 – 284	37	63.36	578 – 598
18	1278.4	285 – 296	38	996.46	599 – 618
19	56.745	297 – 313	39	596.29	619 – 630
20	1340.5	314 – 323	-	-	-

Table S2: List of the 33 parameters included in the Morris screening method

No.	Parameter	Input file	Description	Range	Perturbation Method	Reference
1	SFTMP	*.bsn	Snowfall temperature (℃)	[-5, 5]	Replace	(Khorashadi Zadeh et al., 2017; Li et al., 2021; Muleta, 2012; Neitsch et al., 2011; Zhang et al., 2013)
2	SMTMP	*.bsn	Snowmelt base temperature (℃)	[-5, 5]	Replace	(Li et al., 2021; Neitsch et al., 2011; Zhang et al., 2013)
3	SMFMX	*.bsn	Melt factor for snow on June 21 (mm H_2O/℃-day)	[0, 20]	Replace	(Li et al., 2021)
4	SMFMN	*.bsn	Melt factor for snow on December 21 (mm H_2O/℃-day)	[0, 20]	Replace	(Li et al., 2021)
5	TIMP	*.bsn	Snowpack temperature lag factor	[0.01, 1]	Replace	(Li et al., 2021; Neitsch et al., 2011; Zhang et al., 2013)
6	SURLAG	*.bsn	Surface runoff lag coefficient	[0.05, 24]	Replace	(Li et al., 2021; Zhang et al., 2013)
7	GW_DELAY	*.gw	Groundwater delay time (days)	[0, 500]	Replace	(Hernandez-Suarez and Nejadhashemi, 2022; Jeong et al., 2024; Mao et al., 2024)
8	ALPHA_BF	*.gw	Base flow alpha factor	[0, 1]	Replace	(Hernandez-Suarez and Nejadhashemi, 2022; Khorashadi Zadeh et al., 2017; Li et al., 2021; Mao et al., 2024; Zhang et al., 2013)
9	GWQMN	*.gw	Threshold depth of water in the shallow aquifer required for return flow to occur (mm H_2O)	[0, 5000]	Replace	(Hernandez-Suarez and Nejadhashemi, 2022; Jeong et al., 2024; Li et al., 2021)
10	GW_REVAP	*.gw	Groundwater "revap'' coefficient	[0.02, 0.2]	Replace	(Jeong et al., 2024; Li et al., 2021; Neitsch et al., 2011; Zhang et al., 2013)

11	REVAPMN	*.gw	Threshold depth of water in the shallow aquifer for ‘‘revap’’ or percolation to the deep aquifer to occur (mm H_2O)	[0, 1000]	Replace	(Hernandez-Suarez and Nejadhashemi, 2022; Jeong et al., 2024)
12	RCHRG_DP	*.gw	Deep aquifer percolation fraction	[0, 1]	Replace	(Jeong et al., 2024; Khorashadi Zadeh et al., 2017; Li et al., 2021; Neitsch et al., 2011; Zhang et al., 2013)
13	GW_SPYLD[a]	*.gw	Specific yield of the shallow aquifer (m^3/m^3)	[0, 0.4]	Replace	
14	SLSUBBSN[b]	*.hru	Average slope length (m)	[0.75, 1.25]	Factor	(Zhang et al., 2013)
15	HRU_SLP[b]	*.hru	Average Slope steepness (m/m)	[0.75, 1.25]	Factor	(Mao et al., 2024)
16	OV_N[b]	*.hru	Manning’s “n” value for overland flow	[0.75, 1.25]	Factor	(Mao et al., 2024)
17	LAT_TTIME	*.hru	Lateral flow travel time (days)	[0, 180]	Replace	(Jeong et al., 2024; Zhang et al., 2013)
18	CANMX	*.hru	Maximum canopy storage (mm H_2O)	[0, 100]	Replace	(Jeong et al., 2024; Li et al., 2021; Zhang et al., 2013)
19	ESCO	*.hru	Soil evaporation compensation factor	[0.01, 1]	Replace	(Hernandez-Suarez and Nejadhashemi, 2022; Li et al., 2021; Mao et al., 2024; Neitsch et al., 2011; van Griensven et al., 2006)
20	EPCO	*.hru	Plant uptake compensation factor	[0.01, 1]	Replace	(Hernandez-Suarez and Nejadhashemi, 2022; Li et al., 2021; Mao et al., 2024; Neitsch et al., 2011; van Griensven et al., 2006)
21	BIOMIX	*.mgt	Biological mixing efficiency	[0, 1]	Replace	(Hernandez-Suarez and Nejadhashemi, 2022; Khorashadi Zadeh et al., 2017; Zhang et al., 2013)

22	CN2[b]	*.mgt	Runoff curve number multiplicative factor	[0.75, 1.25]	Factor	(Hernandez-Suarez and Nejadhashemi, 2022; Zhang et al., 2013)
23	CH_N2	*.rte	Manning's "n" value for the main channel	[0, 0.3]	Replace	(Mao et al., 2024)
24	CH_K2	*.rte	Effective hydraulic conductivity in main channel alluvium (mm/h)	[0, 500]	Replace	(Hernandez-Suarez and Nejadhashemi, 2022)
25	ALPHA_BNK	*.rte	Baseflow alpha factor for bank storage (days)	[0, 1]	Replace	(Zhang et al., 2013)
26	SOL_Z[b]	*.sol	Soil profile total depth multiplicative factor	[0.75, 1.25]	Factor	(Hernandez-Suarez and Nejadhashemi, 2022; Zhang et al., 2013)
27	SOL_BD[b]	*.sol	Moist bulk density (Mg/cm^3)	[0.75, 1.25]	Factor	(Zhang et al., 2013)
28	SOL_AWC[b]	*.sol	Available water capacity multiplicative factor	[0.75, 1.25]	Factor	(Zhang et al., 2013)
29	SOL_K[b]	*.sol	Saturated hydraulic conductivity multiplicative factor	[0.75, 1.25]	Factor	(Mao et al., 2024; Zhang et al., 2013)
30	SOL_ALB[b]	*.sol	Moist soil albedo.	[0.75, 1.25]	Factor	(Zhang et al., 2013)
31	TLAPS	*.sub	Temperature lapse rate (°C/km)	[-10, 10]	Replace	(Khorashadi Zadeh et al., 2017; Li et al., 2021)
32	CH_K1	*.sub	Effective hydraulic conductivity in tributary channel (mm/h)	[0, 300]	Replace	(Phetanan et al., 2024)
33	CH_N1	*.sub	Manning's "n" value for the tributary channels	[0.01, 30]	Replace	(Phetanan et al., 2024)

[a]The parameter GW_SPYLD is not active in the SWAT model but was included as a dummy parameter to validate the effectiveness of Morris method.

[b]Parameters adjusted using a multiplicative factor are denoted as the "Factor method" to account for spatial variability. All other parameters were adjusted by direct replacement of old values with new ones, denoted as the "Replace method".

References

Hernandez-Suarez, J. S. and Nejadhashemi, A. P.: Probabilistic Predictions of Ecologically Relevant Hydrologic Indices Using a Hydrological Model, Water Resources Research, 58, https://doi.org/10.1029/2021wr031104, 2022.

Jeong, H., Lee, B., Kim, D., Qi, J., Lim, K. J., and Lee, S.: Improving estimation capacity of a hybrid model of LSTM and SWAT by reducing parameter uncertainty, Journal of Hydrology, 633, https://doi.org/10.1016/j.jhydrol.2024.130942, 2024.

Khorashadi Zadeh, F., Nossent, J., Sarrazin, F., Pianosi, F., van Griensven, A., Wagener, T., and Bauwens, W.: Comparison of variance-based and moment-independent global sensitivity analysis approaches by application to the SWAT model, Environmental Modelling & Software, 91, 210-222, https://doi.org/10.1016/j.envsoft.2017.02.001, 2017.

Li, M., Di, Z., and Duan, Q.: Effect of sensitivity analysis on parameter optimization: Case study based on streamflow simulations using the SWAT model in China, Journal of Hydrology, 603, https://doi.org/10.1016/j.jhydrol.2021.126896, 2021.

Mao, H., Wang, C., He, Y., Song, X., Ma, R., Li, R., and Duan, Z.: Advancing SWAT model calibration: A U-NSGA-III-based framework for multi-objective optimization, Water, 16, https://doi.org/10.3390/w16213030, 2024.

Muleta, M. K.: Model performance sensitivity to objective function during automated calibrations, Journal of Hydrologic Engineering, 17, 756-767, https://doi.org/10.1061/(asce)he.1943-5584.0000497, 2012.

Neitsch, S. L., Arnold, J. G., Kiniry, J. R., and Williams, J. R.: Soil and Water Assessment Tool Theoretical Documentation Version 2009, Texas Water Resources Institute. Available electronically from https://hdl.handle.net/1969.1/128050, 2011.

Phetanan, K., Hong, S. M., Yun, D., Lee, J., Chotpantarat, S., Jeong, H., and Cho, K. H.: Enhancing flow rate prediction of the Chao Phraya River Basin using SWAT-LSTM model coupling, Journal of Hydrology: Regional Studies, 53, 101820, https://doi.org/10.1016/j.ejrh.2024.101820, 2024.

van Griensven, A., Meixner, T., Grunwald, S., Bishop, T., Diluzio, M., and Srinivasan, R.: A global sensitivity analysis tool for the parameters of multi-variable catchment models, Journal of Hydrology, 324, 10-23, https://doi.org/10.1016/j.jhydrol.2005.09.008, 2006.

Zhang, C., Chu, J., and Fu, G.: Sobol's sensitivity analysis for a distributed hydrological model of Yichun River Basin, China, Journal of Hydrology, 480, 58-68, https://doi.org/10.1016/j.jhydrol.2012.12.005, 2013.